Nonlinear Normal Modes of a Curved Beam and its Response to Random Loading

Christopher I. VanDamme[1] and Matthew S. Allen[2]

[1]Graduate Student; e-mail: cvandamme@wisc.edu
[2]Associate Professor; e-mail: matt.allen@wisc.edu
University of Wisconsin-Madison: Department of Engineering Physics
1500 Engineering Drive
Madison, Wi 53706

Abstract

Hypersonic vehicles are exposed to high amplitude, random, broadband loading and so, in order to predict the life of the system, the geometrically nonlinear response of certain skin panels must be computed for a long time duration. This is a costly procedure when using the finite element (FE) method due to large mesh sizes and small time step requirements. Nonlinear Reduced Order Models (NLROMs) provide an accurate and computationally efficient alternative to compute the response of such structures. The NLROMs still require computationally expensive validation that is conventionally done by comparing responses with the full FE model. An alternative approach to validating NLROMs is to compute their Nonlinear Normal Modes (NNMs), which are independent of the loading scenario and provide information regarding the system's response over a range of energy or response amplitude. This work investigates the relationship between the NNMs and response of a curved beam to random inputs. The structure contains quadratic and cubic nonlinearities that produce both a softening and hardening behavior of the beam as the system energy is increased. A connection is made between the accuracy of NNMs computed from NLROMs and their random response predictions.

Keywords: Reduced Order Modeling, Geometric Nonlinearities, Nonlinear Normal Modes, Finite Element Analysis, Structural Dynamics

1 Introduction

In order to develop high performance hypersonic vehicles design must be implemented that exploit geometrically nonlinear response. Exploiting nonlinearities in the design of thin structural members can lead to significant weight reduction [1, 2]. The utilization of nonlinear design requires nonlinear analysis methods to accurately predict the response of the skin panels. The implementation of nonlinear analysis techniques for hypersonic vehicles comes at a significant computational cost due to the extreme loading conditions experienced during their flight trajectories. The loading environment of the vehicle skin panels is non-deterministic due to the random broadband loading associated with the aeroacoustic pressure fields and thermal loads [1]. In order to accurately model the response statistics of the vehicles the equations of motion must be integrated over a long time. It is straightforward to account for geometric nonlinearity in the FE (finite element) method, and most commercial codes implement this. However, to accurately model the skin panels for concept aircraft, large and detailed meshes are needed to generating a large system of equations that need to be integrated for each time step. The combination of nonlinear analysis techniques, large equations of motion and numerical integration over a long time duration creates a bottleneck for design-analysis cycles.

An alternative to computing the nonlinear response of the full FE model is to generate a nonlinear reduced order model (NLROM). The motion of the structure is represented with a small number of basis vectors that describe the response while retaining the nonlinearities. NLROMs greatly reduce the number of degrees of freedom (DOF) from potentially millions in the FEM to a small subset of amplitudes. Not only do the NLROMs reduce the number of DOF, but the numerical integration of the NLROM is no longer constrained by the minimum time step requirement of the FE model. The time step is determined by the maximum frequency of modal coordinate within the basis set of the NLROM which generally provides a larger allowable time step in comparison to the full FE model.

Although NLROMs have been shown to accurately predict the response of various structures [1, 3, 4, 5, 6, 7] it is not always a straightforward process to generate them and validation is still required for each new design that a NLROM is generated for. The conventional method of validating NLROMs is to compare load dependent time history responses with the full FE model. This remains a costly procedure because it requires one to simulate the response of the full FE model for each loading scenario of interest; just because the NLROM has been shown to produce the same response as the full FEM for one loading it does not guarantee that it will have similar accuracy for other loading scenarios. There is a need for the development of a validation procedure for NLROMs that is independent of the loading scenario. The development of such a validation procedure will aid in the reduction of design-analysis cycles.

Nonlinear Normal Modes (NNMs) may provide a solution to load independent NLROM validation for random response analysis. Previous works on both flat and curved geometrically nonlinear structures have shown promise in validation of NLROMs using NNMs [8, 9, 10]. In addition, prior work investigating the connection between NNMs and the random response of a structure found that different NLROMs could be understood in terms of the NNMs that they capture and the associated modal coupling [11]. This finding proved to correspond with the part of the frequency spectrum that each NLROM captured accurately. That work was for a flat structure which only showed hardening response. This work explores whether this holds for curved structures, where softening happens and modal coupling is more significant. In addition, this work seeks to bridge a connection between accuracy metrics based on NNMs and accuracy of the NLROMs' random response predictions. It will be shown that there is a tight connection between the accuracy of a model's NNMs (using these metrics) and the accuracy of the response predicted by the model in a random loading environment.

2 Theory

The geometrically nonlinear elastic FE equation of motion for N degree-of-freedom (DOF) system can be written as

$$\mathbf{M}\ddot{\mathbf{x}} + \mathbf{C}\dot{\mathbf{x}} + \mathbf{K}\mathbf{x} + \mathbf{f}_{NL}(\mathbf{x}) = \mathbf{f}(t) \tag{1}$$

where $\mathbf{M}$, $\mathbf{C}$ and $\mathbf{K}$ are the mass, damping and linear stiffness matrices respectively of dimension N $\times$ N. The displacement, velocity acceleration vectors $\mathbf{x}$, $\dot{\mathbf{x}}$ and $\ddot{\mathbf{x}}$ are N $\times$ 1 vectors. The nonlinear restoring force term $\mathbf{f}_{NL}$ is a function of the displacements of the system. The external vector, $\mathbf{f}(\mathbf{t})$ can be both a random function of space and time resulting in a N $\times$ 1 vector for each point in time. Equation (1) represents a second order nonlinear stochastic differential equation (SDE). This nonlinear SDE is commonly written in the form of the Fokker-Planck equation [12] which has a closed form solution for only a few low order systems. Although there are attempts to approximate closed form solutions for higher order systems the only reliable, universally valid way of solving this equation is to numerically integrate the system and perform statistical analysis on the results.

The system represented in Eq (1) can be reduced to a NLROM to efficiently solve for the statistical response of the system. The first step in the creation of the NLROM is to identify the basis vectors to be used in the NLROM, these will consist of the linear mode shapes of the structure. Neglecting the damping, external forces and nonlinear restoring force terms in Eq (1) the linear modes of the model are found by solving the eigenvalue problem of the linear system

$$\left(\mathbf{K} - \omega^2\mathbf{M}\right)\phi_{\mathbf{r}} = \mathbf{0} \tag{2}$$

which can be solved to find the coordinate transformation represented as

$$\mathbf{x}(t) = \Phi_m \mathbf{q}(t) \tag{3}$$

where Φ_m is the N $\times$ m the mass normalized mode matrix comprised of the mode vectors, ϕ_r, and $\mathbf{q}$ is the m $\times$ 1 vector of time-dependent modal displacements. The motivation for representing the linear equation of motion in this fashion is that the modal coordinates and mode shape matrix are able to accurately predict the response of the system while significantly reducing the number of DOF.

When substituting the modal transformation presented in Eq (3) into the non-linear equation of motion in Eq (1) and then pre-multiplying by Φ^T, where ^{T} is the transpose operator, the r^{th} nonlinear modal equation becomes

$$\ddot{q}_r + c_{\mathbf{r}}\dot{q}_r + \omega_r^2 q + \theta_r(q_1, q_2, ..., q_m) = \phi_r^{\mathbf{T}}\mathbf{f}(\mathbf{x}, \mathbf{t}) \tag{4}$$

where the nonlinear restoring force, θ_r , is represented as a function of the modal displacements by

$$\theta_r(\mathbf{q}) = \phi_r^{\mathbf{T}}\mathbf{f}_{NL}(\Phi_m\mathbf{q}) \tag{5}$$

In [1] it was shown that the restoring forces for a linear elastic system with geometric nonlinearities can be accurately approximated as

$$\theta_r(\mathbf{q}_1,\mathbf{q}_2,...,\mathbf{q}_m) = \sum_{i=1}^{m}\sum_{j=1}^{m} \mathbf{B}_r(i,j)\mathbf{q}_i\mathbf{q}_j + \sum_{i=1}^{m}\sum_{j=1}^{m}\sum_{k=1}^{m} \mathbf{A}_r(i,j,k)\mathbf{q}_i\mathbf{q}_j\mathbf{q}_k \tag{6}$$

where the nonlinear restoring force is a function of quadratic and cubic polynomials with coefficients B_r and A_r respectively for the r^{th} nonlinear modal equation. The primary difference between the various reduced order modeling schemes is the method in which the nonlinear coefficients presented in Eq (6) are estimated.

The method utilized in this work to generate NLROMs is the Implicit Condensation and Expansion (ICE) method. The method applies a series of static forces in the shapes of the linear modes to the FEM each of which would excite only one mode of the linear FEM. The general equation for a forcing with multiple modes can be given as

$$\mathbf{F}_l = \mathbf{M}(\phi_1\hat{\mathbf{f}}_1 + \phi_2\hat{\mathbf{f}}_2 + \ldots + \phi_m\hat{\mathbf{f}}_m) \tag{7}$$

where $\mathbf{F}_l$ is the vector of applied forces, $\mathbf{M}$ is the mass matrix and $\mathbf{f}_r$ is the scaling factor for the modal force. The mass matrix is included above to exploit orthogonality, so that the shapes $\phi_r\hat{\mathbf{f}}_r$ each only excite one mode of the linear system [9]. The displacements due to each set of applied forces are calculated from the FEM and transformed to the modal domain using the basis vectors. The nonlinear stiffness coefficients presented in Eq (6) are then computed using a least squares fit [1].

2.1 Nonlinear Normal Modes

Nonlinear Normal Modes are used in two ways in this work: they are used to evaluate the accuracy of the NLROMs generated as well as used to draw connections with the random response of the full FE model. In linear analysis models are commonly represented by the linear normal modes (LNM) of the structure; they represent the characteristic dynamic properties of system containing the natural frequencies and mode shapes. The extension of LNMs into the nonlinear regime are Nonlinear Normal Modes. The notion of NNMs was first introduced by Rosenberg in 1960s as "a vibration in unison of the system" [13]. The definition was later relaxed by Kerschen et al. to state it as a "a not necessarily synchronous periodic solution of the conservative, nonlinear equations of motion" [14]. The NNMs in this work will be plotted on a frequency energy plot (FEP) to show how the resonance frequency changes with energy of the system. The NNMs of the undamped and unforced NLROMs as represented in Eq (4) are computed in this work using a pseudo arc-length continuation method developed in [15]. The continuation algorithm uses the linear mode shape to initiate the branch for each NNM of the system. From there the algorithm finds a branch of solutions that satisfy the shooting function presented in Eq (8).

$$\mathbf{H}(\mathbf{T},\mathbf{q}_0,\dot{\mathbf{q}}_0) = \begin{Bmatrix} \mathbf{q}(\mathrm{T},\mathbf{q}_0,\dot{\mathbf{q}}_0) \\ \dot{\mathbf{q}}(\mathrm{T},\mathbf{q}_0,\dot{\mathbf{q}}_0) \end{Bmatrix} - \begin{Bmatrix} \mathbf{q}_0 \\ \dot{\mathbf{q}}_0 \end{Bmatrix} = \{\mathbf{0}\} \tag{8}$$

The variables T , $\mathbf{q}_0$, and $\dot{\mathbf{q}}_0$ are the period of integration, initial modal displacements, and initial modal velocities respectively.

3 Numerical Case Study: Curved Beam

The numerical case study for this work is a curved beam which contains quadratic and cubic nonlinearities. The system was modeled using the FE method and various NLROMs were generated to investigate the system. The NLROMs differ based on which linear modes are used in the basis set and what load factors are used to extract the nonlinear stiffness terms. NNMs were computed for each NLROM and checked for convergence to evaluate if the NLROM was accurate. Selected NLROMs are presented to compare with the full order FE model. The random response of both the FE model and the NLROMs was computed to draw correlation between the accuracy of random response and the NNM solutions computed from the NLROMs.

3.1 Curved Beam Finite Element Model

The numerical study is conducted on a finite element model of a curved beam with dimensions as shown in Figure 1 and properties defined in Table 1. The structure was modeled using 255 S4 shell elements in Abaqus® resulting in a total of 1530 DOF. The curved beam has clamped-clamped end conditions and for reference the maximum height, h, of the beam is 0.02 (in) which is equal to the beam thickness. This is a very shallow curvature, such as might occur due to manufacturing imperfections or thermal expansion. For this work the environment of interest is taken to consist of a uniformly distributed pressure (psi) that varies randomly with time such that its power spectral density is constant from [0-1000] Hz.

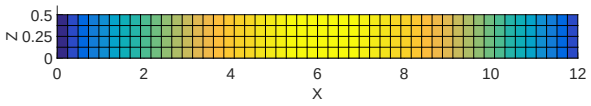

(a) Top Down View of Curved Beam's FE Mesh

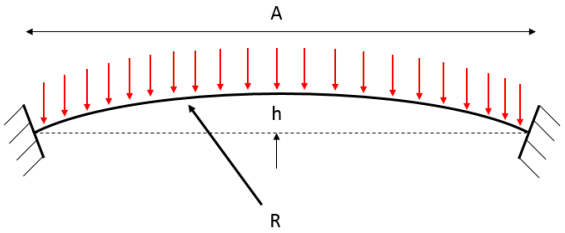

(b) Curved Beam Geometry

Figure 1: Curved Beam Mesh and Geometry

Length (A)	Width	Thickness	Radius of Curvature (R)	Young's Modulus	Density	Poisson's Ratio
12 (in)	0.5 (in)	0.02 (in)	900 (in)	2.97e7 (psi)	7.358e-3 $\left(\frac{lbf}{in^3}\right)$	0.29

Table 1: Table of curved panel dimensions and mechanical properties

The linear mode shapes of curved beam are presented in Figure 2 where they are seen to be similar to those of a flat beam but now the symmetric bending modes include some axial components. The 1st, 3rd, 5th, and 9th modes are symmetric bending modes while the 2nd, 4th, 7th and 11th are anti-symmetric modes. The 6th, 10th and 8th modes, which are not shown, are the first two torsional modes and out of plane bending mode of the curved beam. The natural frequencies of the first 11 linear normal modes of the system are presented in Table 2 along with the damping ratios that result from mass and stiffness proportional damping.

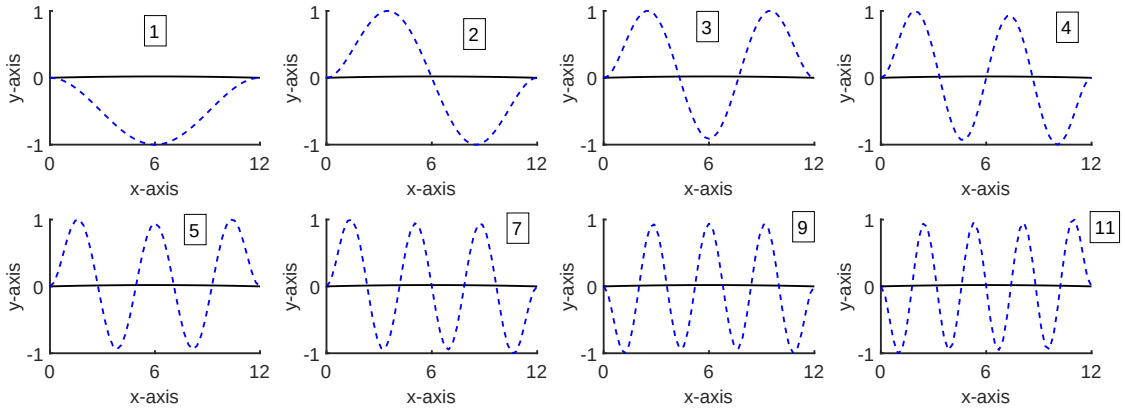

Figure 2: Linear Mode Shapes of the Curved Beam FE Model

3.2 NLROM Generation and Validation

This work will follow the procedure presented in [10] to generate NLROMs of the curved beam. Since the loading environment contains frequencies up to 1000 Hz the linear modes that should be included within the basis set are the symmetric in-plane bending modes within the frequency loading range because they will be directly excited by the external load. One must also

Mode #	Type	Frequency (Hz)	Damping Ratio (ζ)
1	S-Bending	41.22	0.0093
2	A-Bending	79.81	0.0049
3	S-Bending	157.52	0.0028
4	A-Bending	260.63	0.002
5	S-Bending	391.61	0.0018
6	Torsional	425.65	0.0018
7	A-Bending	550.54	0.0019
8	O-Bending	712.11	0.0021
9	S-Bending	738.83	0.0021
10	Torsional	851.45	0.0023
11	A-Bending	957.60	0.0025

Table 2: Curved Beam Natural Frequencies
Variable Designation: S - Symetrix, A - Anti-symetric, O - Out of plane

include modes that are statically coupled to the linear modes, i.e. the modes that are excited when the structure is forced into the shape of a linear mode at high amplitude. The modes that are statically coupled to a mode in question can be found by applying a force in the shape of a mode using $\mathrm{f} = \mathbf{M}\phi$ to the nonlinear FE model and observing the response of each mode. In Figure 3 the modes that are statically coupled to the first mode (symmetric) and second mode (anti-symmetric) are presented for a range of forcing amplitudes. The legend for each figure shows the modes that have the largest static coupling in descending order. This information aids in determining which modes should be included within the basis set next if the NLROM has not converged.

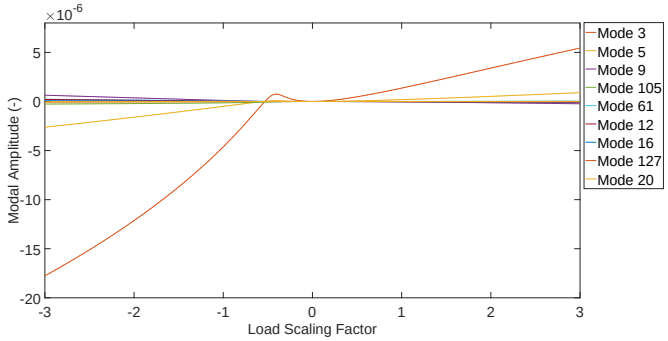

(a) Amplitude of each linear modal coordinate when a force is applied in the shape of the first linear mode.
(First mode is omitted to show other modes in more detail)

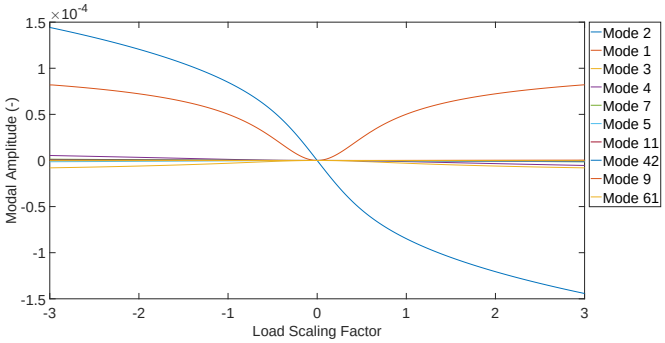

(b) Amplitude of each linear modal coordinate when a force is applied in the shape of the second linear mode.

Figure 3: Identification of Statically Coupled Modes to the First and Second Modes

NLROM	Linear Modes
NLROM_1	[1]
NLROM_2	[1, 3, 5]
NLROM_3	[1-5, 9, 12]
NLROM_4	[1-5, 7, 9, 11, 12, 16]

Table 3: NLROMS Generated and the Linear Modes used within each Basis Set

In order to evaluate how the addition of basis vectors to the system changes the nonlinearities, an initial NLROM was generated using only the 1st mode and then additional modes were added to monitor how the system behavior changes. This was evaluated by checking convergence of computed NNMs for each NLROM as basis vectors were added. The NNMs provide insightful information as to how the system behaves as the energy of the system increases. Since the loading is a uniform pressure the mode that will be primarily excited is the first mode so only the 1st NNM will be considered here. The 1st NNM was computed for each NLROMs shown in Table 3 and and the resulting frequency energy plots are shown in Figure 4. It is seen that all of the NNMs show a similar softening of the system initially as energy increases followed by a hardening behavior. The significant difference between these NLROMs is their tendency to divert towards the internal resonance at 45 Hz. $NLROM_2$ and $NLROM_3$ follow the internal resonance and using the algorithm in [15] the NNM solutions were not able to find a branch that returned to the primary backbone. $NLROM_3$ deviates even further from $NLROM_2$ and follow another internal resonance at 70 Hz. With the addition of the several symmetric and anti-symmetric modes to the basis set the NNM computation was able to revert back to the main backbone curve for $NLROM_4$.

At each of the points marked with red dots in Figure 4, the initial displacement of the structure (corresponding to the solution at that frequency and energy) was plotted and is shown in subplot(b) of Figure 4. This reveals which modes are active at each point on the NNM; when the deformation shape differs significantly from the shape of the first linear mode it can bed inferred that modal interactions are important. The NNM found for $NLROM_2$ is found to be dominated by an interaction with Mode 5, while the NNM for $NLROM_3$ is dominated by mode 7.

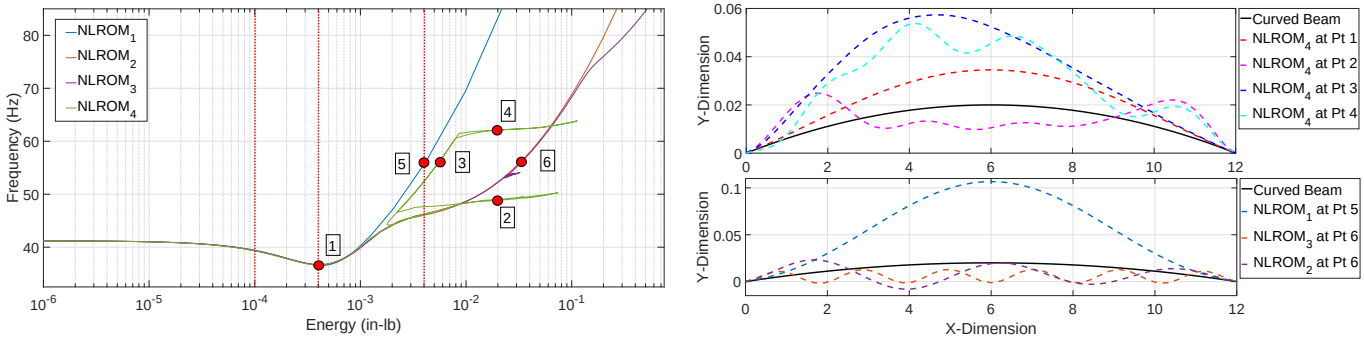

(a) 1st NNM Computed for Various NLROMs

(b) 1st NNM Solutions Projected onto the FE Model

Figure 4: Convergence of 1st NNM

To check whether the NLROMs had converged on a true NNM of the finite element model, the solutions were checked at various points on the NNM curves by using them as an initial condition in the full finite element model and checking whether the resulting response was periodic. The periodicity of the system is defined as

$$\varepsilon = \frac{\|\mathbf{x_T} - \mathbf{x_0}\|}{\|\mathbf{x_0}\|} \tag{9}$$

where T is the period of NNM solution, $\mathbf{x_0}$ is the initial displacement vector computed from the NLROM and $\mathbf{x_T}$ is the displacement vector after one period of integration computed from the full FE model. If the solution is periodic then the NNM predicted by the NLROM satisfies the full FE model and the NLROM is accurate in the vicinity of that NNM. The red dashed vertical lines represent the energy levels at which periodicity checks were performed. Energy is used to determine solution points for this work because, as will be discussed later, a connection can be made between the distribution of energy present in a random response and NNMs.

To graphically represent what the periodicity checks are evaluating the NNM solution point 3 depicted in Figure (4) for $NLROM_4$ is used and projected onto the FEM shown in Figure (5) . Subplot (a) shows the time history response over the period of integration for a set of nodes where each line represents the vertical displacement of a node; subplot(b) shows the projection of the physical displacements onto the modal domain using Eq (10) to investigate modal basis vectors contributing to the response. This allows for identification of modes that may have significant contribution but are not included within the basis set. The legend in subplot(b) of each figure represents the ranking of the modal contributions to the response.

$$\mathbf{q}(\mathrm{t}) = \Phi^{\mathrm{T}} M x(\mathrm{t}) \tag{10}$$

The time history shows a symmetric response over the period of integration which coincides with a periodic solution as represented numerically by a computed periodicity value of $\varepsilon = 0.033$ for a maximum displacement of the FE model of 0.0633" which is greater than three times the thickness of the beam. This is within the strongly nonlinear regime for geometrically nonlinear structures. The modal amplitude plot shows that the NLROM consists of the major contributing modes (1-5, 9, 7, 11, 12, 16). The next most important modes are modes 42, 19, 61, etc..., but their response is small relative to the modes that are already included in the basis. The NLROMs generated and presented in this section will be used in Section 3.4 to draw comparisons between the accuracy of NNM solutions and the accuracy of their random response predictions.

Table 4 presents the periodicity values calculated for each NLROM at each of the energy values. From Table 4 it is seen that NLROM_1 provides the least accurate prediction of the NNM solution since the large values of ε indicate that the response is far from periodic NLROM_2 has the most accurate prediction of the NNM even though it tend to divert down the internal resonance branch and never returns to the main backbone of the system. NLROM_3 and NLROM_4 provide similar accuracy for similar levels of displacement even though the NNMs found from these NLROMs were vastly different from those found for NLROM_2. It cannot be guaranteed that NLROM_2 or NLROM_3 are valid along the backbone of the system because the NNM solutions were unable to trace the path. The same statement is true for NLROM_4, it is not guaranteed that along the internal resonance branch that NLROM_2 and NLROM_3 follow that the NLROM is valid. Unfortunately, its is not yet known whether it is important that a NLROM can accurately predict internal resonance branches, when the ultimate goal is to compute the random response.

Energy Value	NLROM_1		NLROM_2		NLROM_3		NLROM_4	
	ε	x_{max}	ε	x_{max}	ε	x_{max}	ε	x_{max}
1e-4	0.0038	0.010	0.001	0.011	0.0025	0.0121	0.003	0.0118
3e-4	0.0344	0.018	0.0028	0.021	0.0046	0.0215	0.005	0.0227
4e-3	0.2328	0.0612	0.0170	0.0538	0.02217	0.0542	0.0264	0.0597

Table 4: Periodicity (ε) and Maximum Displacement of FEM for NNM Solutions Computed for each NLROM

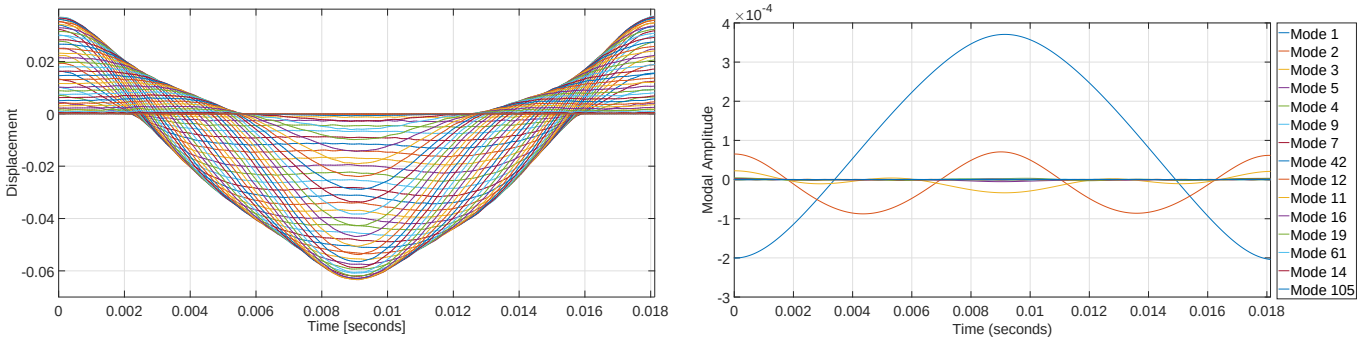

(a) Time History Response over one Period

(b) Modal Time History Response over one Period

Figure 5: Periodic Solution Point from NNM 1

3.3 Random Response of Finite Element Model

The full FE model and NLROMs were subjected to random forces at various levels, each defined by a constant density, S_0. The desired and generated spectral input for the case of $S_0 = 1e^{-6}$ is presented in Figure (6) which shows that the signal has a constant power distribution over the frequency range of 0-1000 Hz.

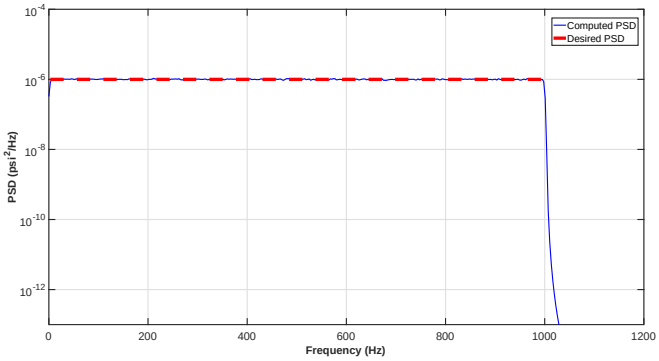

Figure 6: Random Amplitude Power Spectral Density Plot

The input densities, S_0 , for each load case are presented in Table 5 along with the the input variance values, σ_0. The input variance is calculated by integrating the spectral density function over the range of frequencies (in this case from 0 to 1000 Hz) via

$$\sigma_0 = \int_{\omega_1}^{\omega_2} f(\omega) d\omega \tag{11}$$

Load Case	Input Density (S_0)	Input Variance (σ_0)
1	$1e^{-9}$	$1e^{-6}$
2	$1e^{-8}$	$1e^{-5}$
3	$1e^{-7}$	$1e^{-4}$
4	$1e^{-6}$	$1e^{-3}$

Table 5: Input Density Values and Standard Deviations of Input

A mass and stiffness proportional damping model was used to generate a damping matrix for the FE model represented as

$$\mathbf{C} = \alpha\mathbf{M} + \beta\mathbf{K} \tag{12}$$

with $\alpha = 4.77$ and $\beta = 7e-7$. The α and β damping coefficients were calculated using damping of $\zeta = 0.0093$ for the 1st mode and $\zeta = 0.0025$ for the 9th mode. The damping ratios along with the critical element size for an explicit time integration scheme resulted in a time step of $1e^{-7}$ seconds. The random response of the FE model was simulated for 25 seconds with a history output sampling frequency of 50 kHz. The PSD of the full FE model from [0-300] Hz is shown in Figure 7 to show the behavior of the structure's low frequency modes, primarily the first 3 modes of the system. The linear natural frequencies of the system are represented by the vertical dashed lines.

3.4 Comparison of NNMs and Random Response

The first question one may ask is whether the evolution of frequency and energy in the NNM is relevant to the random response. Comparing Mode 1 in Figure 4 with the corresponding peak in the PSD in Figure 7, one can see that both show an initial softening of the system, 6 Hz, followed by a hardening. This trend is seen in the PSDs of the first mode shown Figure 7 where the maximum PSD amplitude for softens 6 Hz as the input density is increased to $S_0 = 1e^{-7}$ then hardens for $S_0 = 1e^{-6}$.

One of the main purposes of the NLROM is to predict the response PSD in a random environment, so it is informative to compare the true PSD from the full FE model with that obtained from the NLROM. The comparison of the response PSDs for the FE model and NLROM$_4$ are presented in Figure 8. The NLROM is accurate for input densities $S_0 = 1e^{-8}$ and $S_0 = 1e^{-7}$ which is up to a moderately nonlinear regime (a RMS displacement of the center node of the beam equal to 1x beam thickness). In addition it is noticed that PSDs computed from the FE model deviated from those computed by the NLROM near the 5th mode at 720 Hz. Since the NNMs for the 5th and 7th mode were not checked it cannot be guaranteed that the NLROM was

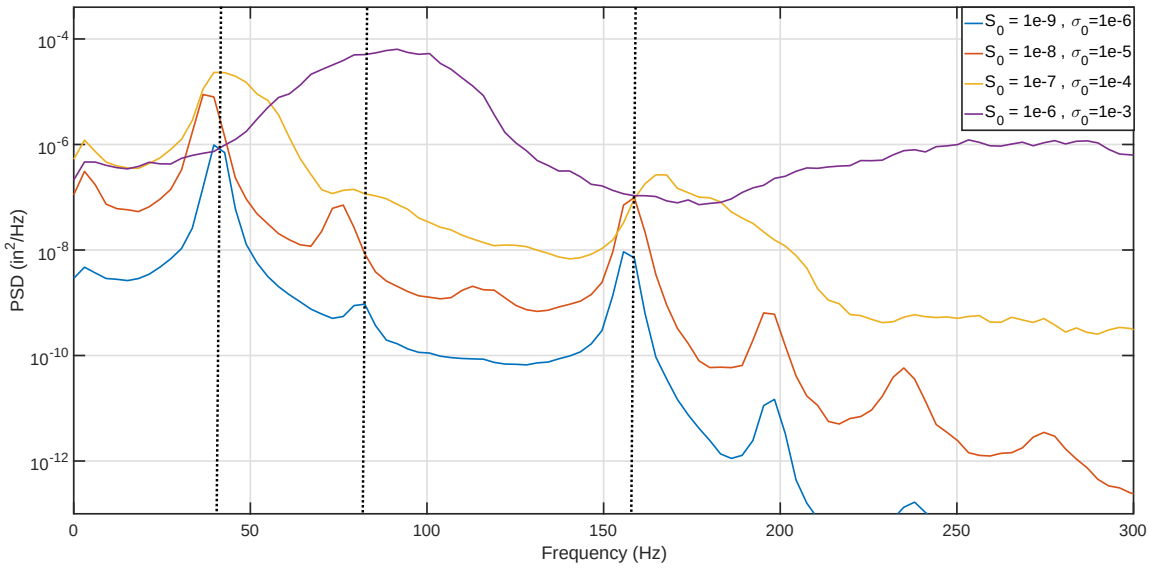

Figure 7: PSDs of Full FEM

accurate for those modes. For the load case where the input density is $S_0 = 1e-6$ the NLROM's prediction of the FE model's PSD decreases in accuracy. The FE model shows a larger hardening of the system and a greater spread of energy across the frequencies as compared to NLROM$_4$ for the first few modes.

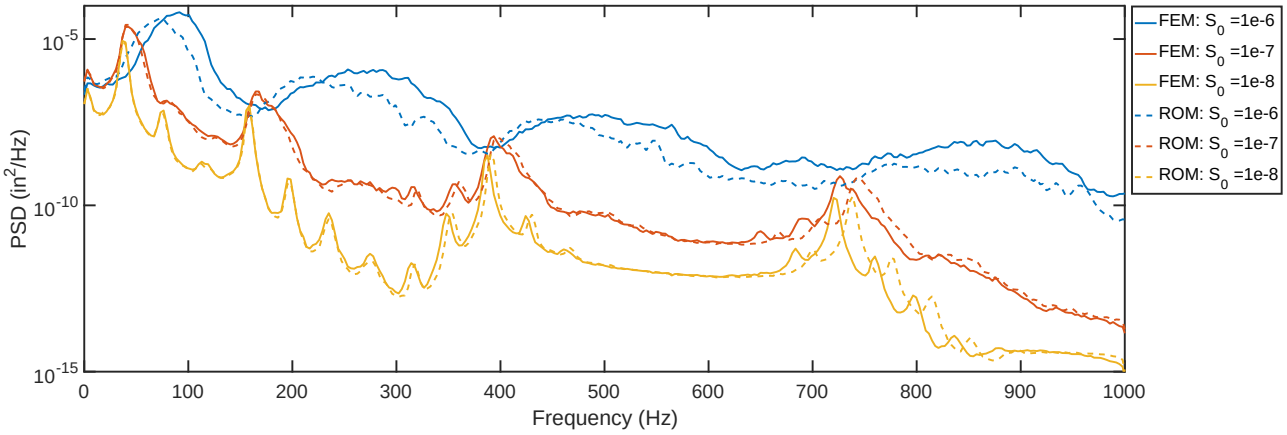

Figure 8: PSDs of NLROM(1-5, 7, 9, 12, 16) and Full FE Model

To establish a quantitative comparison between the NNMs computed from the NLROMs and the accuracy of their random response predictions, a statistical analysis of the NLROMs' response was conducted. The time history of the response from the NLROM was used to compute the probability density functions (PDFs) of the system's energy, which was found to be approximately log-normal. This was repeated for each load level and the estimated distributions are shown in Figure 9. Two standard deviations, denoted 2σ in this work, of the energy distribution was used to estimate an upper bound on energy in the model for each load case and are presented as dashed vertical lines in the figure. The upper bound energy value is used to estimate the highest energy to which each NNM is activated. The assumption in place is that each mode will at some times contain all of the energy in the system. This is based upon the equipartition theorem [16].

In Figure 9 the upper bound of the energy distributions are projected onto the frequency-energy plot of the 1st NNMs computed from the NLROMs. The NNM solutions corresponding to those energy levels are then used to evaluate the accuracy of the NLROMs based upon the periodicity metric in Eq (9). The periodicity values act as a measure of accuracy of the NLROM

prediction of the full FE model with regards to the NNM so they provide a strong measure to correlate with random response prediction error. This was performed for each of the 2σ percentile energy levels shown in Figure 9 for each NLROM. The calculated 2σ upper bound of the energy distribution for each load case and the associated periodicity values of each NNM is presented in Table 6.

For each NLROM the periodicity value representing the inaccuracy of NNM solution increases with increasing energy. NLROM_1 was found to provide the worst periodicity predictions as expected from the earlier results in the validation section. NLROM_2 and NLROM_3 provide similar NNM accuracy values. These values will be used to compare with the error of the NLROMs predictions of the response to the random load.

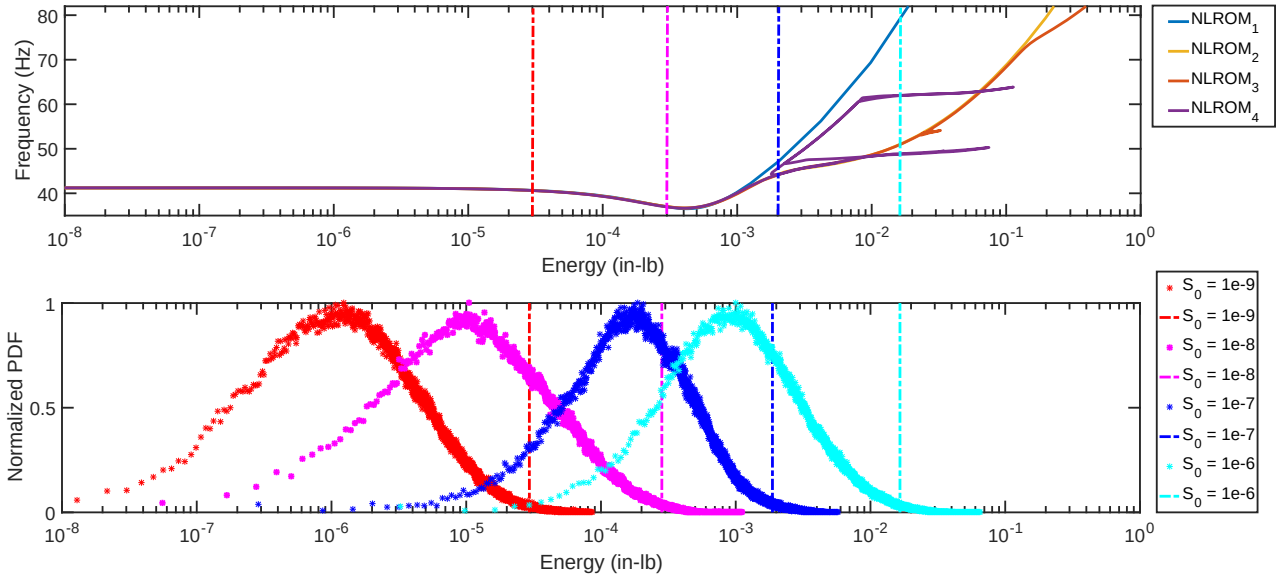

Figure 9: Energy Comparison of NNMs with NLROM Response Data

Input Density: S_0	$2\sigma(E)$	ε : Eq (9)			
		NLROM_1	NLROM_2	NLROM_3	NLROM_4
$1e^{-9}$	3.5e-5	0.00064	0.0014	0.0017	0.0018
$1e^{-8}$	0.00028	0.0344	0.0028	0.0046	0.0033
$1e^{-7}$	0.00187	0.0716	0.0253	0.0081	0.0137
$1e^{-6}$	0.01655	0.175	0.1870	0.1723	0.25

Table 6: Periodicity Values for each NLROM at Upper Bound Energy Levels for each Load Case

The energy of the system was used to provide a connection between random response of the NLROM and the accuracy of a NNM solution. This provides information as to the level that an NNM solution can be expected to be excited for a given load input in a nonlinear random system. Now in order to provide useful information into the response of the system to determine stress statistics required to estimate fatigue life, an accurate estimation of the curved beam's displacement is required. For design of structures for fatigue the common statistical response variables of interest are the root mean square (RMS) and standard deviations of the displacement. Those measures will be used in this work to compare the NLROM predictions with the full FE model for each load case. The connection will be drawn between the accuracy of an NNM solution for a specific energy of the random system and the accuracy of the system response predictions.

The RMS and the upper bound 2σ of the center node displacement of curved beam are presented in Table 7 for the FE model and NLROM_4 predictions. The NLROM provides accurate results up to weakly nonlinear response with input $S_0 = 1e^{-8}$

providing an error in the RMS estimate of 0.003% and an error of 1.18% for the two standard deviation prediction. The NLROM maintains accurate predictions for $s_0 = 1e^{-7}$ load case. The NLROM predictions are within 3% of the FEM for both metrics. As the the input density is increased to $S_0 = 1e^{-6}$ the error of the NLROM increased to 15.6 % for a RMS displacement of the center node of 0.0507 (approximately 2.5x beam thickness), which is strongly nonlinear response. The PDFs of the response at two nodes in the FE model are presented in Figure 10 to graphically represent the comparison of displacement predictions between NLROM$_4$ and full FE model. The PDFs show that NLROM$_4$ provides accurate representation of the FE model with an input density of $S_0 = 1e^{-7}$for both the center node vertical displacement and quarter-span node vertical displacement but losses accuracy for $S_0 = 1e^{-6}$.

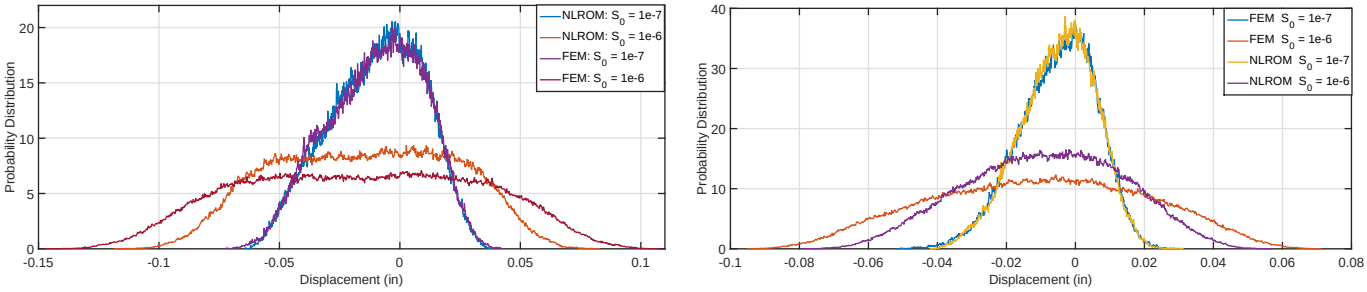

(a) Probability Distribution of Center Node

(b) Probability Distribution of Quarter-Span Node

Figure 10: Probability Distributions of Center Node and Quarter-Length Node: Comparison of FEM with NLROM(#)

Input Density: S_0	RMS$_{\text{FEM}}$	RMS$_{\text{NLROM,4}}$	RMS$_{\%\text{Error,4}}$	$2\sigma_{FEM}$	$2\sigma_{NLROM,4}$	$2\sigma_{\%ERROR,4}$
$1e^{-9}$	0.0025	0.0025	0.001	0.0050	0.0050	0.000
$1e^{-8}$	0.009	0.0091	0.003	0.0170	0.0172	1.18
$1e^{-7}$	0.0222	0.0216	2.7	0.0398	0.0387	2.7
$1e^{-6}$	0.0507	0.0426	15.6	0.0960	0.0732	23.75

Table 7: Comparison of Center Node Vertical Displacement of Curved Beam between FE Model and NLROM$_4$

The percent error of the RMS with respect to the full FE model for all the NLROMs is presented as a bar plot in Figure 11 for the center and quarter-span nodal displacements. It is seen that as the load case increases the accuracy of each NLROM decreases but all are accurate up to $S_0 = 1e^{-7}$. The same trend is seen in the periodicity values presented in Table 6. For both the periodicity and the percent RMS error there is a decrease in accuracy when when loading at $S_0 = 1e^{-6}$. It is seen that the periodicity value for the NNMs computed from the NLROMs evolves approximately in proportion with the RMS error in the random response.

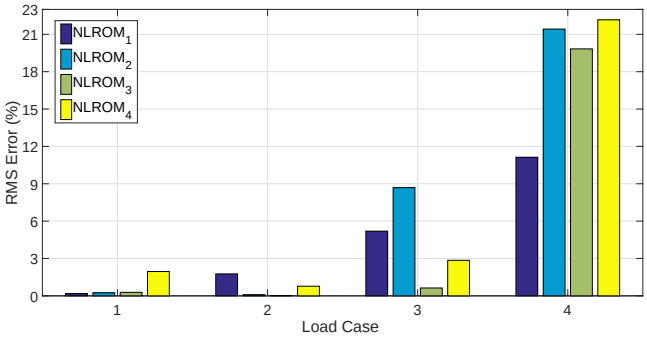

(a) Center Node Vertical Displacement

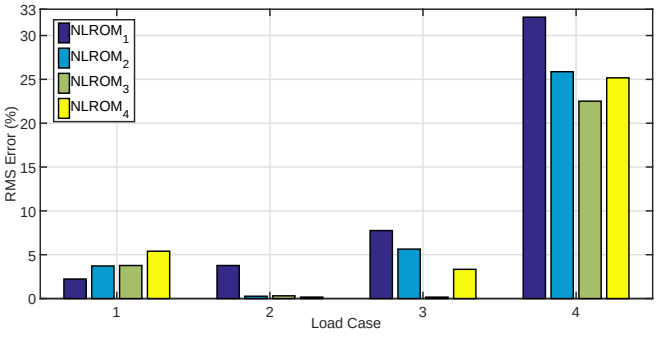

(b) Quarter-Span Node Vertical Displacement

Figure 11: Percent Error in RMS Prediction of Nodal Displacements between the FE Model and NLROMs

4 Conclusion

In this work NLROMs were generated for a curved beam finite element model to investigate the relationship between the system's NNMs and response to random inputs. It was shown that NNMs can provide an alternative measure of accuracy of the nonlinear system that is independent of loading. This was verified by comparing the periodicity of the computed NNMs for each NLROM with the accuracy of the random response predictions at corresponding energy levels. Furthermore, NNMs can predict qualitative behavior that is seen in the random response PSDs such as softening and hardening of the system as was shown by the frequency energy plot of the 1st NNM. This work used a uniform pressure distribution varying randomly in time which primarily excites the low order modes of the system. The next step will be to implement a load that will also randomly vary in spatial distribution along the curved beam. A limiting factor of this work was the ability to compute NNM solutions along all possible branches. It proved to be challenging to compute the NNMs along the primary backbone beyond the internal resonances, and as a result it was not possible to evaluate the accuracy of the NNMs at higher energy levels.

References

[1] R. G. J. Hollkamp, "Reduced-order models for acoustic response prediction," Air Force Research Laboratory, Tech. Rep., 2011.

[2] M. S. A. J. D. Schoneman, "Leveraging geometric nonnonlinear for efficient design of thin beams," in *6th International Conference on Nonlinear Vibrations, Localization and Energy Transfer*, 2016.

[3] X. W. M. M. T. E. S. Spottswood, "Nonlinear reduced order modeling of curved beams: A comparison of methods," *50th AIAA/ASME/ASCE/AHS/ASC Structures, Structural Dynamics, and Materials Conference*, 2009.

[4] S. M. S. J. J. Hollkamp, R. W. Gordon, "Nonlinear modal models for sonic fatigue response prediction: a comparison of methods," *Sound and Vibration*, 2005.

[5] R. W. G. J. J. Hollkamp, "Reduced-order modeling of the random response of curved beams using implicit condensation," AFRL, Tech. Rep., 2006.

[6] S. A. Przekop, A. Rizzi, "Dynamic snap-through of thin-walled structures by a reduced-order method," *AIAA Journal*, vol. 45, no. 10, pp. 2510–2519, 2007.

[7] X. Q. W. M. P. M. R. Perez, ""nonintrusive structural dynamic reduced order modeling for large deformations: Enhancements for complex structures"," *Journal of Computational and Nonlinear Dynamics*, 2014.

[8] R. K. B. D. J. H. M. Allen, "Evaluation of geometrically nonlinear reduced-order models with nonlinear normal modes," *AIAA Journal*, vol. 53, pp. 3273–3285, 2015.

[9] M. Kuether, R. Allen, "Validation of nonlinear reduced order models with time integration targeted at nonlinear normal modes," *Nonlinear Dynamics, Volume 1 Conference Proceedings of the Society for Experimental Mechanics Series*, 2015.

[10] M. A. C.I. Van Damme, "Using nnms to evaluate reduced order models of curved beam," in *Rotating Machinery, Hybrid Test Methods, Vibro-Acoustics & Laser Vibrometry, Volume 8 Conference Proceedings of the Society for Experimental Mechanics Series*, 2016, pp. 457–469.

[11] R. K. J.D. Schoneman, M.S. Allen, "Relationships between nonlinear normal modes and response to random inputs," pp. 184–199, 2017.

[12] S. N. P. Kumar, "Modified path integral solution of fokker-planck equation: respons and bifurcation of nonlinear systems," vol. 5, 2010.

[13] R. M. Rosenberg, "Normal modes of nonlinear dual-mode systems," vol. 27, pp. 263–268, 1960.

[14] A. V. J. C. G. G. Kerschen, M. Peeters, "Nonlinear normal modes, part i: A useful framework for the structural dynamicist," *Mechanical Systems and Signal Processing*, 2009.

[15] G. S. G. K. M. Peeters, R. Virguie, "Nonlinear normal modes, part ii: Toward a practical computation using numerical continuation techniques," *Mechanical Systems and Signal Processing*, 2009.

[16] R. S. L. G. M. Spelman, "Statistical energy analysis of nonlinear vibrating systems," vol. 373, 2015.